Design of a H_2 PSA for cogeneration of ultrapure hydrogen and power at an advanced integrated gasification combined cycle with pre-combustion capture

Design of a H_2 PSA for Cogeneration of Ultrapure Hydrogen and Power at an Advanced Integrated Gasification Combined Cycle with Pre-Combustion Capture

Mauro Luberti, Daniel Friedrich, Stefano Brandani, Hyungwoong Ahn*

Scottish Carbon Capture and Storage Centre

Institute for Materials and Processes, School of Engineering,

The University of Edinburgh, Mayfield Road, Edinburgh, EH9 3JL, UK

*Corresponding author: Hyungwoong Ahn (h.ahn@ed.ac.uk)

Abstract

A novel hydrogen pressure swing adsorption system has been studied that is applied to an advanced integrated gasification combined cycle plant for cogenerating power and ultrapure hydrogen (99.99+ mol%) with CO_2 capture. In designing the H_2 PSA, it is essential to increase the recovery of ultrapure hydrogen product to its maximum since the power consumption for compressing the H_2 PSA tail gas up to the gas turbine operating pressure should be minimised to save the total auxiliary power consumption of the advanced IGCC plant. In this study, it is sought to increase the H_2 recovery by increasing the complexity of the PSA step configuration that enables a PSA cycle to have a lower feed flow to one column for adsorption and more pressure equalisation steps. As a result the H_2 recovery reaches a maximum around 93% with a Polybed H_2 PSA system having twelve columns and the step configuration contains simultaneous adsorption at three columns and four-stage pressure equalisation.

Keywords: IGCC, Pressure swing adsorption, Hydrogen purification, Cogeneration

1. Introduction

Eight refineries in the UK are currently emitting 14.9 $MtCO_2$ which accounts for around 3% of total UK CO_2 emission in 2009 (DECC, 2009). The INEOS refining plant in Grangemouth, for example, emits around 2.2 $MtCO_2$ per annum, which is equivalent to 4% of total CO_2 emissions in Scotland (SEPA, 2008). The Committee on Climate Change (CCC) estimated that there will be a chance to curtail around 3.5 $MtCO_2$ out of 14.9 $MtCO_2$ from refineries by 2030 by improving their energy efficiency. The CCC also foresaw that beyond this target of abatement, a further reduction would be possible by deploying carbon capture units on H_2

plants and replacing combustion fuels with carbon-neutral biomass (Committee on Climate Change, 2011).

It is well known that most refining complexes face a significant deficiency of their existing hydrogen production capacity. Hydrogen is needed for operating their hydrotreating desulphurisation process that removes mainly sulphur and other impurities from raw petroleum products and hydrocracking units for upgrading low-grade heavy residues to more valuable diesel and lube base oil. The need for H_2 is bound to increase due to the trends of 1) more stringent sulphur and nitrogen specification in fuel oils, 2) increasing crack spread, and 3) the rapid change of crude oil properties from 'light and sweet' to 'heavy and sour'. Due to the requirement of very high operational severity in both units for deep desulphurisation and improved product quality, ultrapure hydrogen with a purity of 99.99+ mol% should be utilised for the hydroprocessing. Accordingly, most refineries are forced to increase rapidly their hydrogen production capacities to cope with the increased H_2 demand but it is doubtful that given the upcoming carbon emission regulation conventional steam methane reforming (SMR) H_2 processes would be still the best option to meet this demand.

Most refineries have their own power plant to provide various units with the utilities such as steam and electricity. In particular, when integrated with a carbon capture unit, integrated gasification combined cycle (IGCC) power plants would have significantly lower energy penalty than coal-fired power plants since a carbon capture unit can be applied to a gas stream having higher CO_2 partial pressure in IGCC power plants. As a result, it has been reported that IGCC power plants integrated with pre-combustion capture would have notably higher net power efficiency than coal fired power plants (DOE, 2007).

It should also be noted that IGCC power plants run gas turbines using H_2-rich fuel gas (88 – 91 mol% H_2 purity) in CO_2 capture cases instead of mixtures of CO and H_2 in non-capture cases and it is easy to produce ultrapure hydrogen product by purifying the H_2-rich fuel gas. This means that by replacing both the existing SMR H_2 plant and the coal-fired power plants with an advanced IGCC plant it would be possible to provide refining complexes with ultrapure H_2 and power simultaneously where CO_2 can be inherently captured as depicted in Figure 1.

In producing ultrapure hydrogen (99.99+ mol%) from such a gas mixture as composed of H_2, CO_2, CO, N_2 and Ar, it is well-known that a pressure swing adsorption (PSA) is the only economically feasible, commercialised separation process. The multi-column PSA process, known as UOP Polybed, has been widely applied to SMR H_2 plants to produce ultrapure H_2 from shifted syngas. However, the conventional H_2 PSA has been designed and optimised against a feed stream of around 71% H_2, 19% CO_2, 4% CO and 5% CH_4 at 20 bar found in a SMR H_2 process. This composition and the pressure of the raw H_2 feed in a SMR-based H_2 plant is quite different from the raw H_2 fuel gas in IGCC power plants with carbon capture

(88.75% H_2, 2.12% CO_2, 2.66% CO, 5.44% N_2, 1.03% Ar at 34 bar). Therefore, there is a need to revisit the design of the H_2 PSA process to estimate the H_2 recovery and productivity obtained at the operating conditions to meet the H_2 product purity as high as 99.99+ mol%.

2. Design basis of a H_2 PSA integrated with an IGCC power plant

This study is aimed at the design of a H_2 PSA system that is applicable to an advanced IGCC plant for producing both ultrapure H_2 and power. The advanced IGCC plant is a modification of a conventional IGCC power plant with carbon capture to include a new H_2 PSA unit and its block flow diagram is illustrated in Figure 2.

The process design of the conventional IGCC power plants with carbon capture is based on an exemplary IGCC power plant using a Shell gasifier (DOE, 2007; Kapetaki et al., 2013). The syngas stream from the shift reactors is fed to an acid gas removal unit (AGR), such as a dual-stage Selexol unit, to remove CO_2 as well as H_2S from the syngas. In the conventional IGCC process, the treated syngas leaving the AGR becomes saturated with water in a fuel gas saturation column and then is fed to the combustion chamber of a gas turbine. But in this study the treated syngas is split into two streams: one stream flows directly to a gas turbine for power generation and the other is sent to a H_2 PSA for ultrapure H_2 production. The H_2 PSA tail gas obtained as by-product needs to be compressed up to the operating pressure of the gas turbine and sent to the combustion chamber with the H_2-rich fuel gas.

Various H_2 PSA designs have been studied so far in order to estimate their performance when they are applied to conventional SMR H_2 plants (Ribeiro et al., 2008, 2009; Lopes et al., 2011). Even though the H_2 recovery that is expected of a commercial Polybed H_2 PSA in a SMR H_2 plant is as high as 89 mol%, they could achieve at most 71 mol% H_2 recovery at 99.99+% H_2 purity. This is because the H_2 PSA systems in their design were configured with only four columns while commercial Polybed H_2 PSA systems in most cases contain seven to sixteen adsorption columns to enable enhanced hydrogen recovery. In this study, H_2 PSA systems having up to twelve columns have been simulated to see the effect of different PSA step configurations that are subject to the chosen number of columns on the H_2 recovery using an in-house cyclic adsorption process simulator, hereinafter named CySim (Friedrich et al., 2013).

Given the composition and the pressure of raw H_2 feeds that previous study dealt with (Ahn et al., 2001), it was concluded that H_2 PSA designs that were configured with adsorption columns having two adsorbent layers would exhibit a better performance than those having adsorption columns packed with a single adsorbent. This is because it is unlikely to find a versatile adsorbent that has better working capacities than others for all impurities being contained in a raw H_2 feed. Therefore, a layered bed is usually configured such that an activated carbon layer near the feed end plays a role in adsorbing mainly CO_2

and CH_4 while a zeolite layer on top of the activated carbon layer removes CO and N_2. The length ratio of the carbon to zeolite layers is regarded as one of the key parameters that need to be optimised (Ahn et al., 2001, 2012; Ribeiro et al., 2008; Yang and Lee, 1998; Park et al., 1998). Given the composition of the new raw H_2 feed that has relatively small CO_2 and no CH_4, however, it is plausible that an adsorption column packed with zeolite 5A performs better than those with a layered bed of activated carbon and zeolite 5A.

The production of the H_2 PSA tail gas should be minimised in order to reduce the power consumption relating to its compression before feed to the gas turbine. In this study the aim is to maximise H_2 recovery by adding more columns to the H_2 PSA process to enable more complicated step configurations for minimising the H_2 loss and consumption. To know the maximum hydrogen recovery that a H_2 PSA could achieve is essential in determining the mass balance around the H_2 PSA, i.e. the flowrate and the composition of both ultrapure hydrogen product and PSA tail gas. Once the mass balance is obtained at the condition of maximum H_2 recovery, it is possible to estimate the auxiliary power consumption in compressing the H_2 PSA tail gas and the power generation in the gas and steam turbines accurately.

3. H_2 PSA simulation

The dynamic behaviour of a H_2 PSA is described by a mathematical model which couples mass, momentum and energy balances over a packed bed with the appropriate boundary conditions for each step of the cycle (Friedrich et al., 2013).

Since the flow is assumed to be a dispersed plug flow the component and overall material balances along the column are given by:

$$\frac{\partial c_i}{\partial t} + \frac{(1-\varepsilon)}{\varepsilon} \cdot \frac{\partial \overline{Q}_i}{\partial t} + \frac{\partial (c_i \cdot v)}{\partial z} + \frac{\partial J_i}{\partial z} = 0 \tag{1}$$

$$\overline{Q}_i = \varepsilon_p c_i^m + \rho_p \overline{q}_i \tag{2}$$

$$J_i = -D^L c_T \frac{\partial x_i}{\partial z} \tag{3}$$

$$\frac{\partial c_T}{\partial t} + \frac{(1-\varepsilon)}{\varepsilon} \cdot \sum_i \frac{\partial \overline{Q}_i}{\partial t} + \frac{\partial (c_T \cdot v)}{\partial z} = 0 \tag{4}$$

Since the column undergoes significant temperature excursions over a cycle caused by the heat of adsorption, constitutive energy balances are coupled with the mass balance:

$$\varepsilon \frac{\partial U_f}{\partial t} + (1-\varepsilon)\frac{\partial U_P}{\partial t} + \varepsilon \frac{\partial (H_f \cdot v)}{\partial z} + \frac{\partial J_T}{\partial z} + \sum_{i=1}^{N_c} \frac{\partial (J_i \widetilde{H}_i)}{\partial z} + h_w \frac{A_c}{V_c}(T_f - T_w) = 0 \tag{5}$$

$$\frac{dU_P}{dt} = \varepsilon_P \frac{dU_{P,f}}{dt} + (1-\varepsilon_P)\frac{dU_{P,s}}{dt} \tag{6}$$

$$J_T = -\lambda^L \varepsilon \frac{\partial T_f}{\partial z} \tag{7}$$

In Eq. (5), T_w is assumed to be equal to ambient temperature since a heat balance around the wall is not taken into account.

In this work the adsorption rate is represented by Linear Driving Force (LDF) model for both macropores and micropores.

$$\varepsilon_p \frac{dc_i^m}{dt} + \rho_p \frac{d\bar{q}_i}{dt} = k_i^p \frac{A_p}{V_p}\left(c_i - c_i^m\right) \tag{8}$$

$$k_i^p \frac{A_p}{V_p} = \frac{15 \cdot \varepsilon_p \cdot D_{p,i}}{r_P^2} \tag{9}$$

$$\frac{d\bar{q}_i}{dt} = k_i^{cr} \frac{3}{r_c}\left(q_i^* - \bar{q}_i\right) \tag{10}$$

The axial mass dispersion coefficient D^L and the axial thermal dispersion coefficient λ^L are estimated using the correlations by Wakao and Funazkri (1978):

$$\frac{\varepsilon \cdot D^L}{D_m} = 20 + 0.5 \cdot Sc \cdot \mathrm{Re} \tag{11}$$

$$\frac{\lambda^L}{k_g} = 7 + 0.5 \cdot \mathrm{Pr} \cdot \mathrm{Re} \tag{12}$$

The pressure drop along the column is evaluated using the Ergun equation (Ergun, 1952):

$$-\frac{\partial P}{\partial z} = \frac{150\mu(1-\varepsilon)^2}{d_p^2 \varepsilon^2} v + \frac{1.75\rho_f(1-\varepsilon)}{d_p \varepsilon} v|v| \tag{13}$$

The boundary conditions for the gas phase concentrations and the enthalpies are given by the Danckwerts boundary conditions. With the conventions that the positive flow direction is from 0 (feed end) to L (product end) these can be written in a general form as:

$$J_T\big|_{z=0} = \frac{v+|v|}{2}\left(H_{f,0-} - H_{f,0}\right) \tag{14}$$

$$J_T\big|_{z=L_c} = \frac{v-|v|}{2}\left(H_{f,L_c+} - H_{f,L_c}\right) \tag{15}$$

$$J_i\big|_{z=0} = \frac{v+|v|}{2}\left(c_{i,0-} - c_{i,0}\right) \tag{16}$$

$$J_i\big|_{z=L_c} = \frac{v-|v|}{2}\left(c_{i,L_c+} - c_{i,L_c}\right) \tag{17}$$

Adsorption equilibrium of pure hydrogen, carbon dioxide, carbon monoxide, nitrogen and argon on zeolite 5A are reported in the literature in the range of operating pressures of the H_2 PSA system investigated in this study (Lopes et al., 2009; Hua Ma et al., 1991). The adsorption equilibria are predicted by the following extended dual-site Langmuir model:

$$q_i^* = \frac{q_{i,s}^1 b_i^1 P x_i}{1+\sum_{j=1}^{N_c} b_j^1 P x_j} + \frac{q_{i,s}^2 b_i^2 P x_i}{1+\sum_{j=1}^{N_c} b_j^2 P x_j} \quad (18)$$

$$\text{with } b_i^l = b_{i,0}^l \exp\left(\frac{-\Delta \widetilde{H}_i^l}{RT}\right).$$

Experimental data (Lopes et al., 2009; Hua Ma et al., 1991) are fitted using Origin 8.5 (OriginLab, 2010). The isotherm parameters of dual-site Langmuir model are given in Table 1.

Table 1. Isotherm parameters of dual-site Langmuir model for zeolite 5A.

Gas	$q_{i,s}^1$ (mol/kg)	$q_{i,s}^2$ (mol/kg)	$b_{i,0}^1$ (bar^{-1})	$b_{i,0}^2$ (bar^{-1})	$(-\Delta H_i^1)$ (J/mol)	$(-\Delta H_i^2)$ (J/mol)
CO_2	0.7077	3.711	$1.077\cdot10^{-7}$	$1.233\cdot10^{-4}$	38,312	29,808
H_2	0.7077	3.711	$4.227\cdot10^{-7}$	$1.333\cdot10^{-4}$	19,674	9,282
CO	0.7077	3.711	$2.431\cdot10^{-8}$	$2.321\cdot10^{-5}$	47,736	20,994
N_2	0.7077	3.711	$2.141\cdot10^{-6}$	$8.987\cdot10^{-5}$	31,338	14,956
Ar	0.7077	3.711	$1.399\cdot10^{-9}$	$4.901\cdot10^{-4}$	50,239	11,171

Cycle performances are evaluated according to the common parameters of H_2 purity, H_2 recovery and H_2 productivity defined as follows:

$$H_2\ Purity = \frac{\int_0^{t_{AD}} C_{H_2} u\big|_{z=L} dt}{\sum_i^{N_c} \int_0^{t_{AD}} C_i u\big|_{z=L} dt} \quad (19)$$

$$H_2\ Recovery = \frac{\int_0^{t_{AD}} C_{H_2} u\big|_{z=L} dt - \int_0^{t_{PR}} C_{H_2} u\big|_{z=L} dt}{\int_0^{t_{AD}} C_{H_2} u\big|_{z=0} dt} \quad (20)$$

$$H_2\ Productivity = \frac{\left(\int_0^{t_{AD}} C_{H_2} u\big|_{z=L} dt - \int_0^{t_{PR}} C_{H_2} u\big|_{z=L} dt\right) A_c}{t_{cycle} M_{ads}} \quad (21)$$

The aim is to design a H_2 PSA process having a capacity of 110 H_2 MMSCFD that is approximately equivalent to 1,609 H_2 mol/s. Given the H_2 mole fraction in the raw H_2 feed, the required flowrate of a raw H_2 feed flowing to the H_2 PSA would be around 2,015 mol/s assuming 90% H_2 recovery. According to the design of the IGCC power plant with carbon capture using a Shell dry coal-fed gasifier (DOE Case 6, 2007), the advanced IGCC plant for cogeneration of power and ultrapure hydrogen would be configured such that around 40% of the raw H_2 gas is directed to the H_2 PSA while the remaining 60% flows to a syngas humidifier and subsequently a combustion chamber in the gas turbine just as in the conventional IGCC power plant.

Planning as a future work an experimental campaign to validate the simulation results subsequent to this study, the dimension of adsorption columns in this study was determined to be the same as those of a lab-scale six-column PSA rig as shown in Table 2. Given the column size and dimension, the feed flowrate is set at 0.002 mol/s with a scaling factor of 10^{-6}. The values of other parameters used in the simulation are also presented in Table 2. In all the simulations, the set of the partial and ordinary differential equations and the algebraic equations were solved using the in-house CySim simulator. The discretization method for the spatial domain in the column was central finite difference method (CFDM) with 20 grid points along the column. The system of differential algebraic equations was solved with the DAE solver SUNDIALS (Friedrich et al., 2013).

Table 2. List of column parameters, particle parameters, and operating conditions of H_2 PSA simulations.

Column parameters	
Column length, L_c [m]	0.5
Column internal diameter, D_c [m]	0.025
External bed void fraction, ε [-]	0.391
Axial mass dispersion coefficient, D^L [m^2/s]	$1.165 \cdot 10^{-4}$
Axial thermal dispersion coefficient, λ^L [W/m·K]	1.279
Wall heat transfer coefficient, h_w [$W/m^2 \cdot K$]	95
Adsorbent parameters	
Pellet density, ρ_p [kg/m^3]	1,126
Pellet void fraction, ε_p [-]	0.503
Adsorbent specific heat capacity, $c_{P,s}$ [J/kg·K]	920
Pellet averaged diameter, d_p [mm]	1.70
Macropore LDF coefficient, $k_i^p \cdot A_p/V_p$ $H_2/CO_2/CO/N_2/Ar$ [s^{-1}]	9.222/6.073/7.518/7.897/7.284
Micropore LDF coefficient, $k_i^{cr} \cdot 3/r_c$ $H_2/CO_2/CO/N_2/Ar$ [s^{-1}]	0.7467/0.0017/0.0332/0.1697/0.1800 (Lopes et al., 2009)
Operating conditions	
P_{ads} [bar]	34
P_{des} [bar]	1
T_{feed} [K]	303
Q_{feed} [mol/s]	0.002
Feed composition, $y_{H2}/y_{CO2}/y_{CO}/y_{N2}/y_{Ar}$ [molar]	0.8875/0.0212/0.0266/0.0544/0.0103

4. Simulation results

Five different H_2 PSA systems have been investigated to see the change of H_2 recovery and productivity with different levels of complexity of the step configuration that is subject to the number of columns. The H_2 recovery and productivity obtained at different configurations are compared under the operating condition to meet the specification of the H_2 purity (99.99 mol%) at each configuration. First of all, a four-column H_2 PSA system was simulated and the targeted H_2 purity was obtained at a cycle time of 800 seconds. Since all the simulations were carried out at constant feed flowrate of 0.002 mol/s, the total cycle time became longer as more columns that are identical in size and dimension were added to configure six-, nine- and twelve- column H_2 PSA systems. This is because either more than one column can share the total feed gas for adsorption at the same time or more steps need to be included in one cycle. To evaluate whether or not a simulation reaches its cyclic steady state (CSS), the H_2 purity and recovery at a cycle were compared with those at the previous cycle. It was assumed that a cyclic steady state would be reached if the differences of the H_2 purity and recovery between the new and previous cycles were both less than 10^{-6}.

4.1. Four-column H_2 PSA

A four-column H_2 PSA unit is designed such that a providing purge step is located between the two depressuring pressure equalisation (DPE) steps while the two pressurising pressure equalisation (PPE) steps take place in a row after the purge step as shown in Figure 3. The step configuration was reconstructed referring to the step configuration in the literature (Cassidy, 1980).

In the four-column H_2 PSA simulation, the total cycle time was fixed at 800 seconds with the adsorption step time equivalent to $1/4^{th}$ of the cycle time as shown in Figure 3. The purge flow is generated by reducing the column pressure starting from a pressure at the end of the first DPE step to a pressure that can be chosen at an operator's disposal. The equilibrated pressure at the start (or end) of the second DPE step (or the second PPE step) is subject to how much purge flow is generated during the providing purge step. Accordingly, the equilibrated pressure at the end (or start) of the first DPE step (or the first PPE step) is also affected by the amount of purge flow. The step configuration where the providing purge step is located between the two DPE steps has a clear advantage over a cycle where the providing purge step follows the two DPE steps in that it can increase the purge flowrate to a greater extent since the providing purge step can start at a higher pressure. Therefore, this configuration is capable of controlling the product purity in a wider range without having to change the cycle time. It should be noted that the pressure recovery during the

pressure equalisation in this four-column H_2 PSA would decrease with an increasing purge flowrate since the equilibrated pressure at the end of each pressure equalisation stage is affected by the amount of purge flow as shown in Figure 4. By contrast the pressure recovery can be maintained at a constant level regardless of the change of purge flowrate in the configuration where the providing purge step is located after finishing all the DPE steps.

As shown in Figure 4, the pressure profile of a column over a cycle is varied in response to the use of the different amounts of the purge flow investigated in this study. The actual flowrate of the purge gas flowing between two columns under the providing purge and purge steps respectively must decrease with the step time since the driving force diminishes with decreasing pressure difference between the columns. Therefore, an index of PP/F to quantify the varying purge flow as an average purge flow is introduced in this study. The PP/F denotes the ratio of an average purge flowrate being generated from one column during the providing purge step to a feed flowrate to one column for adsorption during one cycle. Note that the amount of the feed flowing to one column is not the same as the total amount of the feed flowing to a PSA system in case that more than one column share total feed flow. The different numbers of PP/F chosen at the three runs are shown in Figure 4 and Table 3. As expected, the start and end pressures during the providing purge step becomes lower with an increase of the PP/F.

The targeted H_2 purity of 99.99+ mol% is achieved in Run 2 where during the providing purge step the column pressure changes from 21.5 to 17 bar that is equivalent to a PP/F of 0.2. At this operating condition, the H_2 recovery and productivity are 72.68% and 162.67 $mol_{H2}/kg/day$, respectively.

Table 3. Performances of the four-column PSA system at different purge flow rates.

Run	Adsorption time [s]	H_2 purity [%]	H_2 recovery [%]	H_2 productivity [$mol_{H2}/kg_{ads}/day$]
Run 1 (PP/F = 0.1)	200	99.976	75.09	168.06
Run 2 (PP/F = 0.2)	200	99.995	72.68	162.67
Run 3 (PP/F = 0.3)	200	99.999	70.56	157.93

4.2. Six-column H_2 PSA

In the case of six-column H_2 PSA systems, two different step configurations were investigated. The first configuration (Figure 5) features feeding the raw H_2 to two columns at the same time, that is to say, each of two columns receiving half the raw H_2 feed (Malek and Farooq, 1997). Due to two columns being used for adsorption in a cycle, the first configuration cannot accommodate an additional pressure equalisation step but has the two-stage pressure equalisation that is the same as the above-mentioned four-column PSA

system. Contrary to the four-column PSA system, a providing purge step is placed after the two pressure equalisation steps as shown in Figure 5. It is anticipated that the alteration to the step configuration would be capable of improving the H_2 recovery since more pressure can be recovered during the pressure equalisation steps, that is to say, less consumption of pure hydrogen for product pressurisation and the reduced feed flowrate to one column for adsorption enables more efficient use of column due to less ingress of impurities into the product end.

In the second configuration (Figure 6), however, only one column is taken up for high pressure adsorption in a cycle just as in the four-column H_2 PSA. Therefore, it is possible to configure a PSA cycle with three-stage pressure equalisation (Xu et al., 2002). It is generally expected that the more pressure equalisation stages a PSA cycle contains the higher hydrogen recovery can be obtained. This is because less hydrogen product is required during the product pressurisation step since the column can be pressurised to a higher pressure in advance during the PPE steps.

Figure 7 clearly exhibits the change of the pressure profile caused by adding one more pressure equalisation step to a PSA cycle. The first configuration having only two pressure equalisation steps (Figure 7(a)) recovers less pressure during the pressure equalisation steps and consumes more hydrogen product during the product pressurisation step than the second configuration with three-stage pressure equalisation (Figure 7(b)) does.

Table 4. Performance of six-column H_2 PSA simulations.

Run	Adsorption time [s]	H_2 purity [%]	H_2 recovery [%]	H_2 productivity [$mol_{H2}/kg_{ads}/day$]
First configuration (Two-stage pressure equalisation)				
Run 4	600	99.999	78.75	117.51
Run 5	700	99.996	81.98	122.33
Run 6	800	99.994	84.41	125.95
Run 7	900	99.975	86.29	128.75
Second configuration (Three-stage pressure equalisation)				
Run 8	150	99.999	76.11	113.57
Run 9	200	99.997	82.47	123.05
Run 10	250	99.994	86.26	128.71
Run 11	300	99.969	88.79	132.48

As observed in Table 4, the first and second configurations can achieve the targeted H_2 purity (99.99+ mol%) at the cycle times of 2400 and 1500 seconds, respectively (Run 6 and 10). The adsorption time in Run 6 (800 seconds) is more than three times longer than that in Run 10 (250 seconds) even though the feed gas entering one column for adsorption is just

halved in flowrate. This can be explained by two reasons. Firstly, the reduced feed flow to one adsorption column for adsorption prevents the ingress of impurities into the product end so it can allow a cycle to have a longer adsorption time. Secondly, the first configuration with only two-stage pressure equalisation has a better working capacity than the second configuration since its column can be more thoroughly regenerated by a stream having more hydrogen and pressurised by more ultrapure hydrogen during the product pressurisation step and inversely gas streams coming from other columns during the DPE steps to a less extent. Therefore, it implies that the H_2 recovery would increase with more stages of pressure equalisation in a cycle but the working capacity of columns would deteriorate due to purging and pressurising the column with more impure gases.

It is noteworthy that the hydrogen recovery is enhanced around 12% with the addition of two columns from four columns (Run 2) to six columns (Runs 6) only by changing the step configuration in spite of both having the same number of pressure equalisation steps. This change is not only caused by less hydrogen consumption during the product pressurisation step but also the longer adsorption time.

At the operating condition of Run 10, the H_2 recovery increases further up to 86.26% mainly due to enhanced pressure recovery taking place over the three-stage pressure equalisation. The stream leaving the column in the course of reducing the column pressure from 34 bar to 9 bar can be reused for pressurising other columns and significantly lower amount of hydrogen product is required for product pressurisation.

The H_2 productivities of both six-column H_2 PSA configurations are similar but lowered in comparison to that of the four-column H_2 PSA performance at the targeted H_2 purity. The change of the H_2 productivity can be explained with respect to the increasing number of columns (or increasing total amount of adsorbents being utilised) and the increasing H_2 recovery. The reduction of the H_2 productivity from four-column to six-column H_2 PSA is due to the increase of the H_2 recovery being less than the corresponding increase of the amount of adsorbent utilised.

4.3. Polybed H_2 PSA (nine and twelve columns)

As mentioned above as more columns are deployed a higher hydrogen recovery would be anticipated in a H_2 PSA system. In this respect Polybed H_2 PSA processes containing seven to sixteen beds with at least three pressure equalisation steps and at least two columns receiving the feed gas for adsorption have been commercially operating for the purpose of H_2 purification (Yang, 1987). In this study a nine-column eleven-step system is investigated following the step configuration found in the literature (Fuderer and Rudelstorfer, 1976) as shown in Figure 8. Figure 9 shows the pressure profile of the nine-column PSA system over a cycle at its cyclic steady state.

The nine-column eleven-step H_2 PSA system benefits from both reduced feed flowrate to one column and intensified pressure equalisation that each of the two six-column H_2 PSA systems has. The feed flowrate fed to one column for adsorption is reduced to one third of the total feed flowrate since three out of nine columns always work for adsorption at the same time. The product pressurisation step starts at 26 bar and the providing purge step commences at 9 bar both of which are similar to those at the second configuration of six-column H_2 PSA system as shown in Figures 7(b) and 9. This is because both PSA systems contain the same number of stages of pressure equalisation in their cycle.

Finally, a twelve-column thirteen-step H_2 PSA system was investigated in order to increase the H_2 recovery close to its maximum. The step configuration is presented in Figure 10 that was originally shown in a patent (Xu et al., 2003). The step configuration features simultaneous adsorption at three columns, simultaneous providing purge and purge at two columns, and four-stage pressure equalisation. Thanks to one additional pressure equalisation step, the product pressurisation step starts at 27 bar and the providing purge step commences at 7.5 bar as shown in Figure 11.

Table 5 lists the performance of the nine- and twelve- column H_2 PSA systems at their cyclic steady state. The nine-column H_2 PSA system can achieve the targeted H_2 purity at the adsorption step time of 1200 seconds (Run 14). It should be noted that the adsorption step time of the twelve-column H_2 PSA to achieve the targeted H_2 purity (1050 seconds at Run 18) is shorter than that of the nine-column H_2 PSA in spite of the same feed flowrate fed to one column, i.e. one third of the total feed flowrate. This indicates that the column working capacity starts to deteriorate due to more incomplete regeneration by a purge flow having less hydrogen and by pressurising the column with more impure streams coming from other columns during the PPE steps instead of ultrapure hydrogen during the product pressurisation step. Nevertheless, the H_2 recovery still increases from 91.85% at the nine-column H_2 PSA to 92.74% at the twelve-column H_2 PSA. Since the improvement of the H_2 recovery is minimal, the H_2 productivity decreases significantly from 91.41 $mol_{H2}/kg_{ads}/day$ at the nine-column H_2 PSA to 69.15 $mol_{H2}/kg_{ads}/day$ at the twelve-column H_2 PSA.

Table 5. Performance of nine-column and twelve-column PSA simulations.

Run	Adsorption time [s]	H_2 purity [%]	H_2 recovery [%]	H_2 productivity [$mol_{H2}/kg_{ads}/day$]
Nine-column H_2 PSA				
Run 12	800	99.998	87.05	86.64
Run 13	1000	99.996	89.94	89.51
Run 14	1200	99.993	91.85	91.41
Run 15	1300	99.974	92.58	92.14
Twelve-column H_2 PSA				

Run 16	750	99.999	89.11	66.52
Run 17	900	99.996	91.17	68.06
Run 18	1050	99.993	92.74	69.15
Run 19	1200	99.978	93.83	70.04

4.4. Comparison among various PSA cycles

Up to now the H_2 recovery and productivity are compared at the targeted H_2 purity of around 99.99+ mol% among various H_2 PSA cycles having different number of columns and different step configurations. Again the H_2 productivity is reduced with the increasing number of columns while the H_2 recovery improves. All the simulation results are plotted on Figure 12 indicating a clear trade-off between hydrogen purity and recovery.

It is expected that more-than-twelve-column H_2 PSA configuration may improve the H_2 recovery further to more than 93% but given the trend of improving H_2 recovery with the number of columns a further improvement of H_2 recovery would be very limited. In particular, more than five stage pressure equalisation steps may not be necessary since the column pressure at the end of the fourth DPE (or PPE) step in the twelve-column H_2 PSA is very close to that at the end of the third DPE (or PPE) step in the nine-column H_2 PSA systems. Therefore, altering a PSA cycle to have more than five pressure equalisation steps cannot recover a notable pressure nor save the amount of ultrapure hydrogen consumed during the product pressurisation step significantly. In addition, it is likely that the working capacity of the column would be badly affected by incomplete regeneration with purge flow having less hydrogen and pressurisation of the column by more impure gas streams than the pure product streams.

Figure 13 shows the hydrogen mole fraction profile along the column at the end of the adsorption step at the cyclic steady state of all the PSA simulation investigated in this study. It clearly shows that with the reduction of the feed flow to one-column for adsorption from four-column to nine-column through six-column with two-stage pressure equalisation the PSA system allows a cycle to have longer adsorption step time so the H_2 MTZ can progress more to the product end at the end of adsorption step. This results in less H_2 remaining at the end of the adsorption step leading to a higher H_2 recovery. The figure also shows that the twelve-column PSA has a broader H_2 mass transfer zone (MTZ) than the nine-column PSA does due to worse regeneration of the column during the purge step and pressurisation with more impure stream while the column is pressurised.

5. Conclusions

A novel H_2 PSA system to produce ultrapure hydrogen from a raw H_2 gas generated in an advanced IGCC process has been proposed in this study. The advanced IGCC plant where CO_2 is intrinsically captured by a pre-combustion capture unit is capable of cogenerating both power and ultrapure hydrogen more economically. The advanced IGCC plant can be used in oil refineries having difficulty in sourcing ultrapure hydrogen that is required to operate hydrotreaters and hydrocrackers and intending to reduce carbon emission from their hydrogen and power plants.

To know the maximum H_2 recovery that a H_2 PSA can produce from the raw H_2 gas is very important in evaluating the performance of the advanced IGCC plant for cogenerating power and ultrapure hydrogen. This is because the flowrate of PSA tail gas, to be determined by the H_2 recovery, should be compressed up to 34 bar from the purge pressure to get the PSA tail gas fed to the gas turbine along with the fuel gas. Therefore, it is essential to design a H_2 PSA such that its H_2 recovery can be maximised in order to minimise the power consumption relating to tail gas compression.

H_2 PSA in commercial SMR hydrogen plants is capable of achieving around 89% H_2 recovery at the 99.9+% H_2 purity. Compared to the raw H_2 gas in the SMR hydrogen plant, the raw H_2 gas fed to the H_2 PSA in the advanced IGCC plant has a gas composition of higher hydrogen and lower impurities and the higher total pressure at which conditions the H_2 PSA is expected to perform better than the H_2 PSA in a SMR H_2 plant. As expected, the Polybed H_2 PSA having twelve columns achieves 93% H_2 recovery at 99.99+ mol% H_2 purity.

Acknowledgement

We would like to express our gratitude for the financial support from KETEP (Grant No.: 2011-8510020030) and EPSRC (Grants No.: EP/F034520/1, EP/G062129/1, and EP/J018198/1).

Nomenclature

A_c Internal column surface area, m^2

A_p Pellet surface area, m^2

b_i^j Adsorption equilibrium constant of site j for comp. i, bar^{-1}

$b_{i,0}^j$ Pre-exponential adsorption equilibrium constant coefficient of site j for comp. i, bar^{-1}

c_i Gas concentration of component i, mol m^{-3}

c_i^m Gas concentration of component i in the macropore, mol m^{-3}

c_T Total gas concentration, mol m^{-3}

$c_{P,s}$ Specific heat capacity at constant pressure of the adsorbent, J kg^{-1} K^{-1}

D^L Axial mass dispersion coefficient, m^2s^{-1}

D_c Column diameter, m

D_m Molecular diffusivity, $m^2 s^{-1}$

$D_{p,i}$ Macropore diffusivity of component i, $m^2 s^{-1}$

d_p Pellet averaged diameter, m

h_w Heat transfer coefficient at the column wall, W m^{-2} K^{-1}

H_f Enthalpy in the fluid phase per unit volume, J m^{-3}

$\widetilde{H}_i$ Partial molar enthalpy in the fluid phase of component i, J mol^{-1}

$\Delta\widetilde{H}_i^j$ Heat of adsorption of site j for component i, J mol^{-1}

J_i Diffusive flux of component i, mol m^{-2} s^{-1}

J_T Thermal diffusive flux, W m^{-2}

k_g Gas conductivity, W m^{-1} K^{-1}

$k_i^p \cdot A_p/V_p$ LDF mass transfer coefficient of component i in the pellet, s^{-1}

$k_i^{cr} \cdot 3/r_c$ LDF mass transfer coefficient of component i in the crystal, s^{-1}

L_c Column length, m

M_{ads} Adsorbent mass, kg

P Pressure, bar

Pr Prandtl number, [-]

$\overline{q}_i$ Average adsorbed concentration of component i in the crystal, mol kg^{-1}

q_i^* Adsorbed concentration of component iat equilibrium, mol kg^{-1}

$q_{i,s}^j$ Saturation capacity of site j for comp. i, mol kg^{-1}

$\overline{Q}_i$ Average adsorbed concentration of component i in the pellet, mol m^{-3}

Q_{feed} Feed flow rate, mol s^{-1}

R Ideal gas constant J mol^{-1} K^{-1}

Re Reynolds number, [-]

r_c Crystal radius, m

r_p Pellet radius, m

Sc Schimdt number, [-]

t Time, s

t_{cycle} Cycle time, s

T Temperature, K

T_f Fluid temperature, K

T_w Column wall temperature, K

u Velocity, m s^{-1}

U_f Internal energy in the fluid phase per unit volume, J m^{-3}

U_P Internal energy in the pellet per unit volume, J m^{-3}

$U_{P,f}$ Internal energy in the macropore per unit volume, J m^{-3}

$U_{P,s}$ Internal energy in the solid phase per unit volume, J m^{-3}

v Interstitial flow velocity, m s^{-1}

V_c Column volume, m^3

V_p Pellet volume, m^3

x_i, y_i Molar fraction of component i, [-]

z Spatial dimension, m

Greek letters

ε External bed void fraction, [-]

ε_p Pellet void fraction, [-]

λ^L Axial thermal dispersion coefficient, W m^{-1} K^{-1}

μ Viscosity, bar s

ρ_f Fluid density, kg m^{-3}

ρ_p Pellet density, kg m^{-3}

References

Ahn H., Yang J., Lee C.-H., 2001. Effects of feed composition of coke oven gas on a layered bed H_2 PSA process. Adsorption 7: 339-356.

Ahn S., You Y.-W., Lee D.-G., Kim K.-H., Oh M., Lee C.-H., 2012. Layered two- and four-bed PSA processes for H_2 recovery from coal gas. Chemical Engineering Science 68: 413-423.

Cassidy R. T., 1980. Polybed Pressure-Swing Adsorption Hydrogen Processing. ACS Symposium Series, volume 135 chapter 13: pages 247-259.

Committee on Climate Change, Chapter 5: Reducing emissions from buildings and industry through the 2020s, 2011.

DECC, Final Emissions Estimates by Fuel Type and End-User Sector, 2009.

DOE NETL, Cost and Performance baseline for fossil energy plants, 2007.

Ergun S., 1952. Fluid flow through packed columns. Chem. Eng. Prog. 48: 89-94.

Friedrich D., Ferrari M.-C., Brandani S., 2013. Efficient simulation and acceleration of convergence for a dual piston pressure swing adsorption system. Ind. Eng. Chem. Res. 52: 8897-8905.

Fuderer A., Rudelstorfer E., 1976. US Patent 3986849 to Union Carbide Corporation.

Hua Ma Yi, Sun W., Bhandarkar M., Wang J., 1991. Adsorption and diffusion of nitrogen, oxygen, argon, and methane in molecular sieve carbon at elevated pressures. Separation Technology 1: 90-98.

Kapetaki Z., Ahn H., Brandani S., 2013. Detailed process simulation of pre-combustion IGCC plants using coal-slurry and dry coal gasifiers. Energy Procedia 37: 2196-2203.

Lopes F. V. S., Grande C. A., Ribeiro A. M., Loureiro J. M., Evaggelos O., Nikolakis V., Rodrigues A. E., 2009. Adsorption of H_2, CO_2, CH_4, CO, N_2 and H_2O in Activated Carbon and Zeolite for Hydrogen Production. Separation Science and Technology 44: 1045–1073.

Lopes F. V. S., Grande C. A., Rodrigues A. E., 2011. Activated carbon for hydrogen purification by pressure swing adsorption: Multicomponent breackthrough curves and PSA performance. Chemical Engineering Science 66: 303-317.

Malek A., Farooq S., 1997. Study of a six-bed pressure swing adsorption process. AIChE J. 43: 2509-2523.

OriginLab, 2010. Data analysis and graphing software. Origin 8.5.

Park J.-H., Kim J.-D., Yang, R. T., 1998. Adsorber dynamics and optimal design of layered beds for multicomponent gas adsorption. Chemical Engineering Science 53: 3951-3963.

Ribeiro A. M., Grande C. A., Lopes F. V. S., Loureiro J. M., Rodrigues A. E., 2008. A parametric study of layered bed PSA for hydrogen purification. Chemical Engineering Science 63: 5258-5273.

Ribeiro A. M., Grande C. A., Lopes F. V. S., Loureiro J. M., Rodrigues A. E., 2009. Four beds pressure swing adsorption for hydrogen purification: case of humid feed and activated carbon beds. AIChE J. 55: 2292-2302.

SEPA's National Air Quality Report, 2008.

Wakao N., Funazkri T., 1978. Effect of fluid dispersion coefficients on particle-to-fluid mass transfer coefficients in packed beds. Chemical Engineering Science 33: 1375-1384.

Xu J., Weist E. L., 2002. US Patent 6454838 B1 to Air Products and Chemicals Inc.

Xu J., Rarig D. L., Cook T. A., Hsu K. K., Schoonover M., Agrawal R., 2003. US Patent 6565628 B2 to Air Products and Chemicals Inc.

Yang R. T., 1987. Gas separation by adsorption processes. Butterworth Publishers.

Yang J., Lee C.-H., 1998. Adsorption dynamics of a layered bed PSA for H_2 recovery from coke oven gas. AIChE J. 44: 1325-1334.

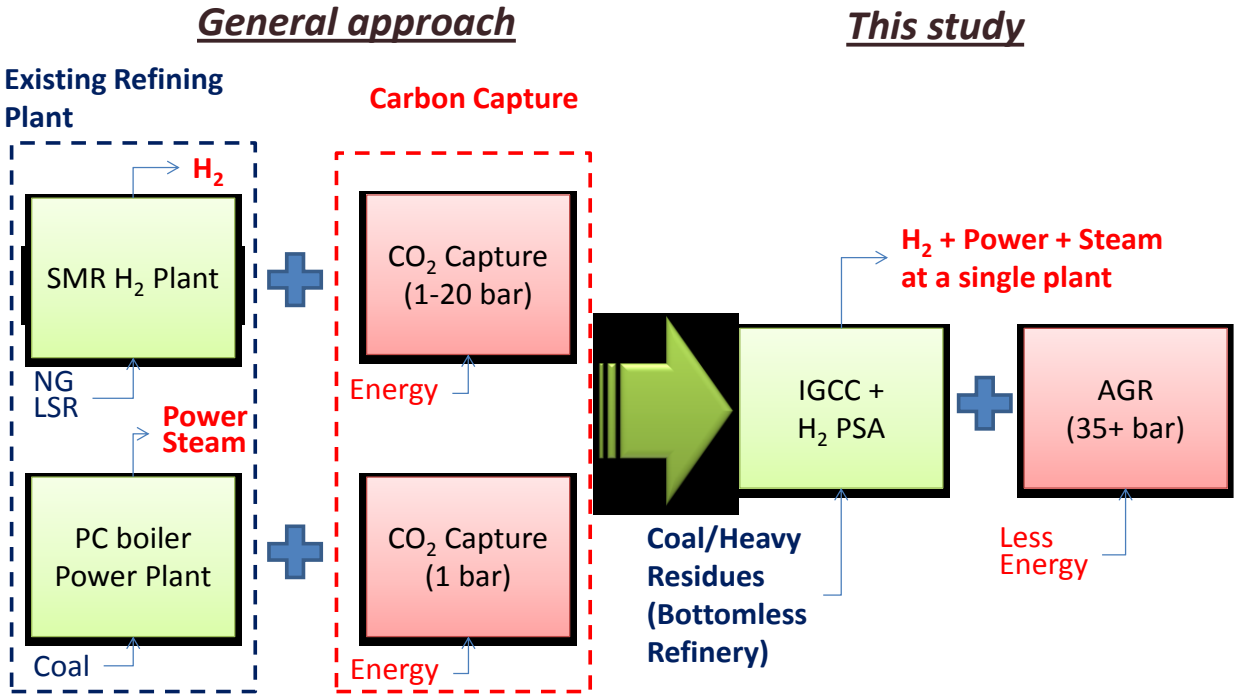

Figure 1. A conceptual diagram to compare general approach to capture CO_2 from a SMR H_2 plant and a coal-fired power plant separately to an advanced IGCC process for cogenerating power and ultrapure hydrogen with carbon capture (this study).

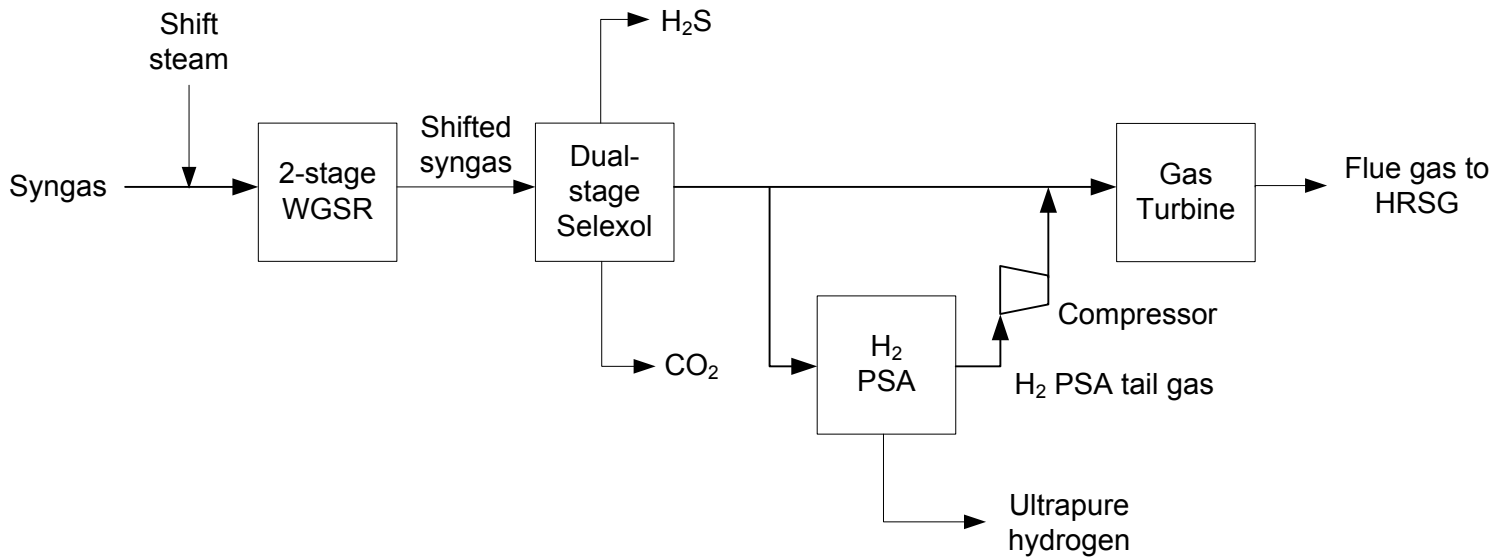

Figure 2. Block flow diagram of an advanced IGCC process for cogenerating power and ultrapure hydrogen.

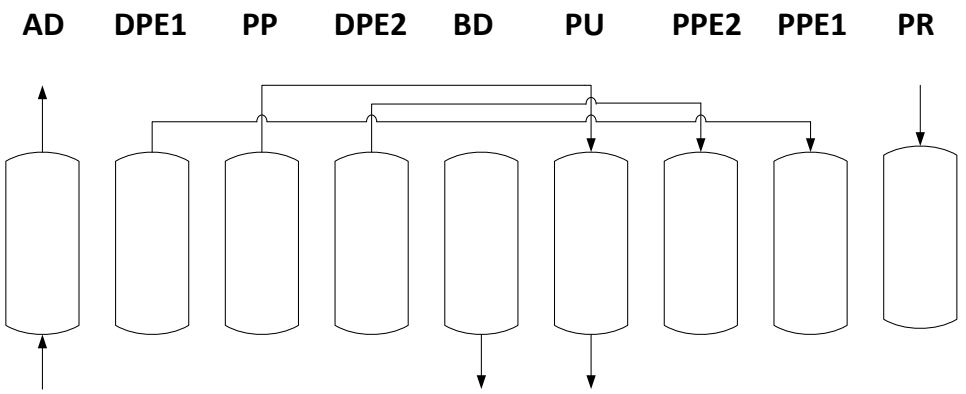

AD			DPE1	PP		DPE2	BD	PU		PPE2	PPE1	PR	
BD	PU	PPE2	PPE1	PR			AD				DPE1	PP	DPE2
DPE1	PP	DPE2	BD	PU		PPE2	PPE1	PR			AD		
PPE1	PR		AD				DPE1	PP		DPE2	BD	PU	PPE2

Figure 3. Step configuration of a four-column PSA cycle (AD: Adsorption, DPE: Depressurising Pressure Equalisation, PP: Providing Purge, BD: Blowdown, PU: Purge, PPE: Pressurising Pressure Equalisation, PR: Product Pressurisation, $t_{AD} = t_{cycle}/4$; $t_{PR} = 3t_{cycle}/16$; $t_{PP} = t_{PU} = t_{cycle}/8$; $t_{BD} = t_{DPE} = t_{PPE} = t_{cycle}/16$).

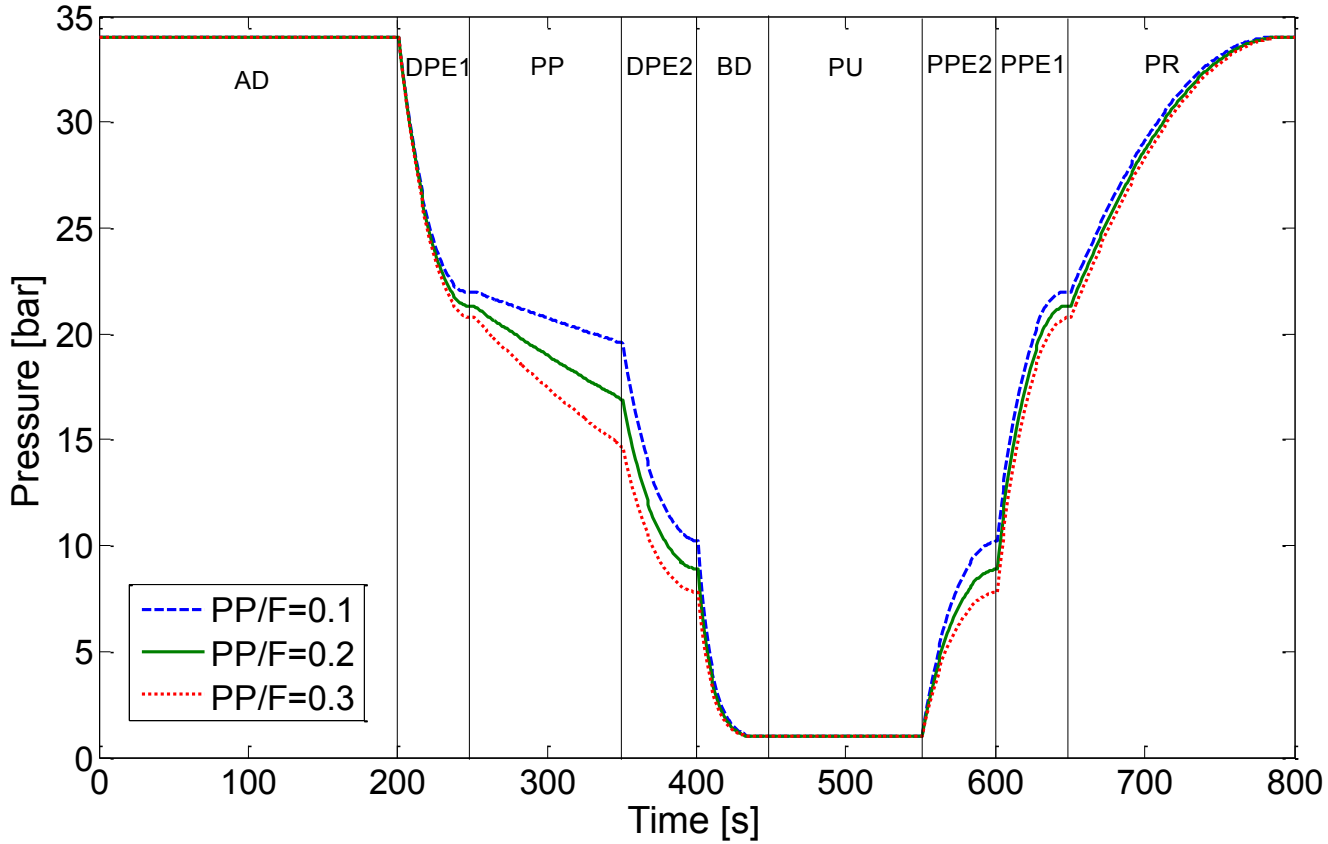

Figure 4. Pressure profiles at the product end of a column over a cycle at the cyclic steady state of the four-column H_2 PSA unit: effect of the different amounts of purge flow.

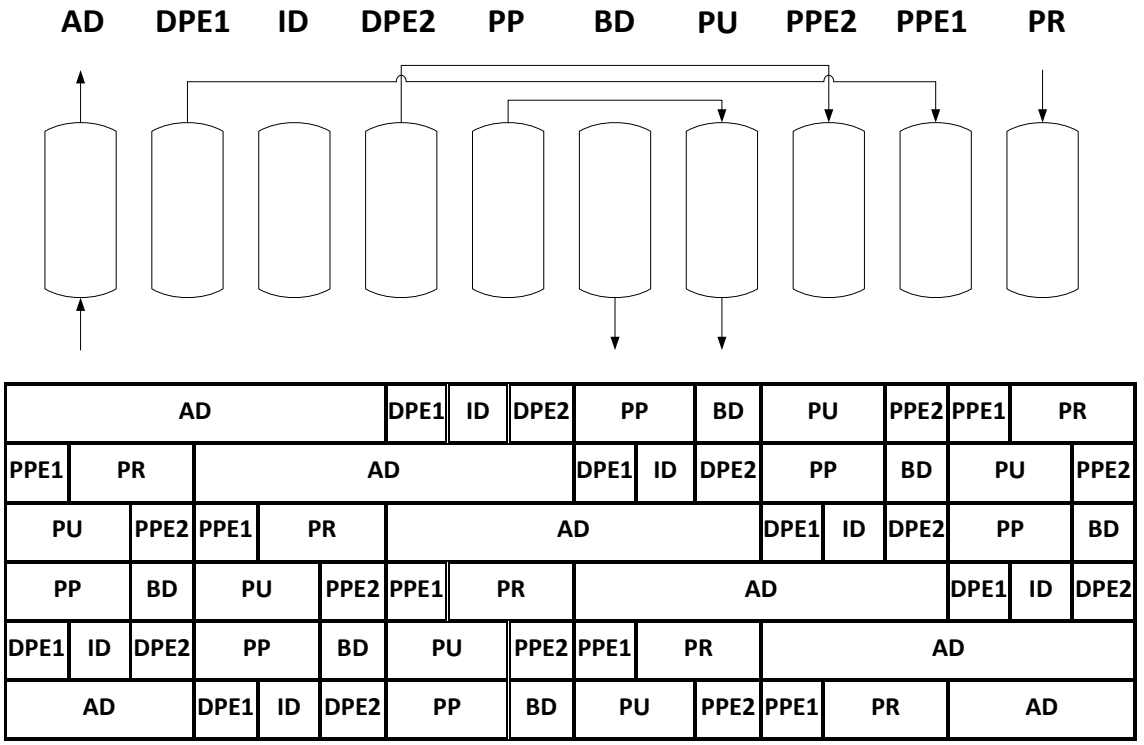

Figure 5. Step configurations of a six-column PSA cycle with two-stage pressure equalisation (AD: Adsorption, DPE: Depressurising Pressure Equalisation, ID: Idle, PP: Providing Purge, BD: Blowdown, PU: Purge, PPE: Pressurising Pressure Equalisation, PR: Pressurisation, $t_{AD} = t_{cycle}/3$; $t_{PP} = t_{PU} = t_{PR} = t_{cycle}/9$; $t_{BD} = t_{DPE} = t_{PPE} = t_{cycle}/18$).

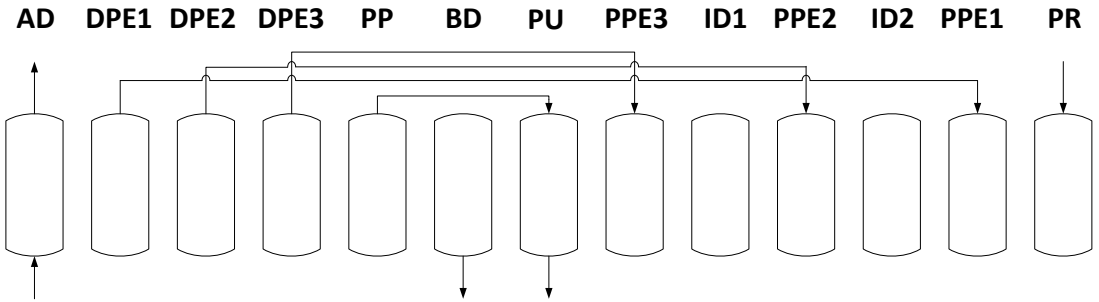

AD			DPE1	DPE2	DPE3	PP		BD	PU		PPE3	ID1	PPE2	ID2	PPE1	PR							
PPE1	PR		AD			DPE1	DPE2	DPE3	PP		BD	PU		PPE3	ID1	PPE2	ID2						
ID1	PPE2	ID2	PPE1	PR		AD			DPE1	DPE2	DPE3	PP		BD	PU		PPE3						
PU		PPE3	ID1	PPE2	ID2	PPE1	PR		AD			DPE1	DPE2	DPE3	PP		BD						
PP		BD	PU		PPE3	ID1	PPE2	ID2	PPE1	PR		AD			DPE1	DPE2	DPE3						
DPE1	DPE2	DPE3	PP		BD	PU		PPE3	ID1	PPE2	ID2	PPE1	PR		AD								

Figure 6. Step configurations of a six-column PSA cycle with three-stage pressure equalisations (AD: Adsorption, DPE: Depressurising Pressure Equalisation, PP: Providing Purge, BD: Blowdown, PU: Purge, ID: Idle, PPE: Pressurising Pressure Equalisation, PR: Pressurisation, $t_{AD} = t_{cycle}/6$; $t_{PP} = t_{PU} = t_{PR} = t_{cycle}/9$; $t_{BD} = t_{DPE} = t_{PPE} = t_{ID} = t_{cycle}/18$).

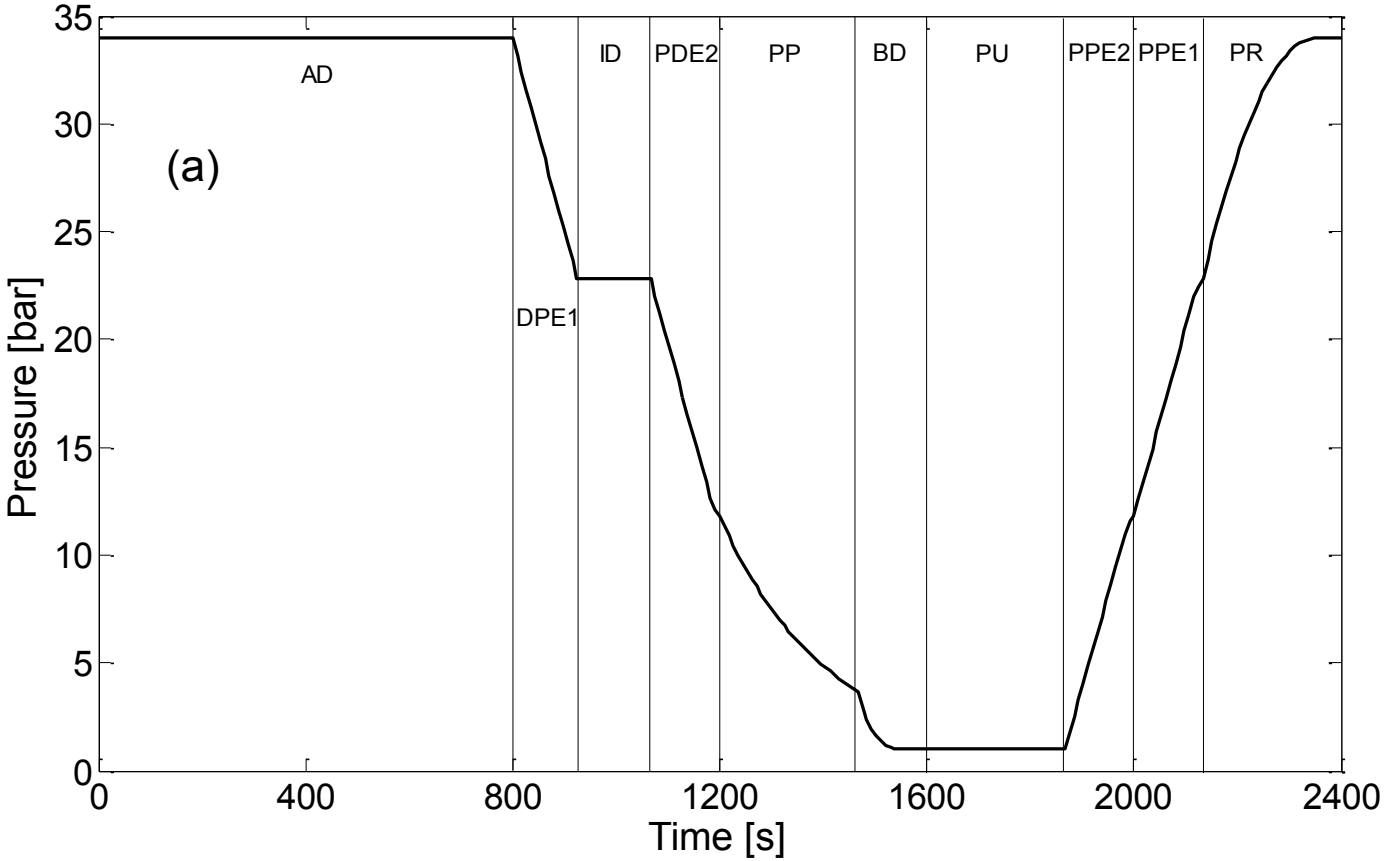
(a)
AD
DPE1
ID
PDE2
PP
BD
PU
PPE2
PPE1
PR
Pressure [bar]
Time [s]
0
5
10
15
20
25
30
35
0
400
800
1200
1600
2000
2400

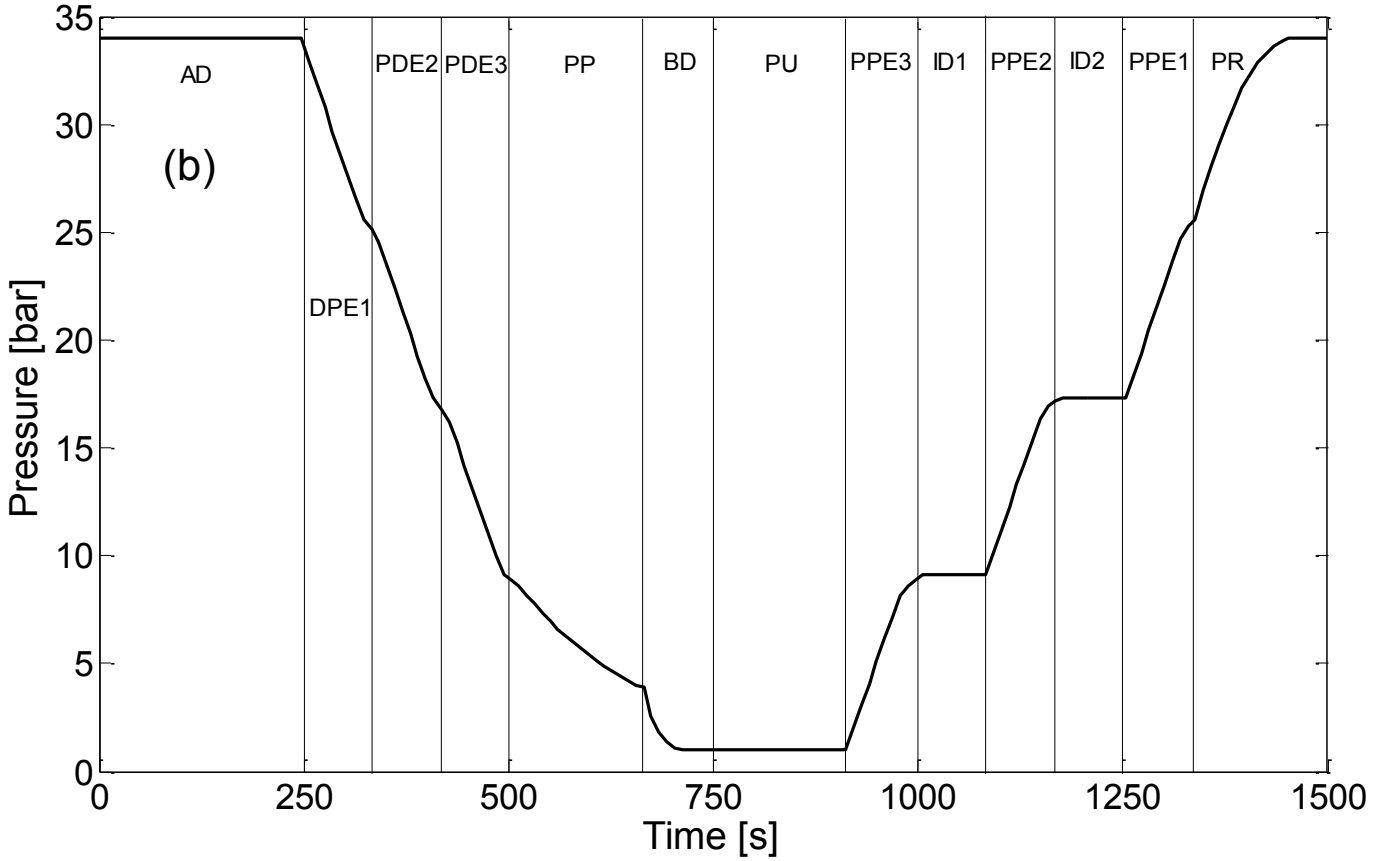

Figure 7. Pressure profiles at the product end of a column over a cycle at the cyclic steady state of six-column H_2 PSA simulations at PP/F = 0.3 with (a) two-stage pressure equalisation (Run 6) and (b) three-stage pressure equalisation (Run 10).

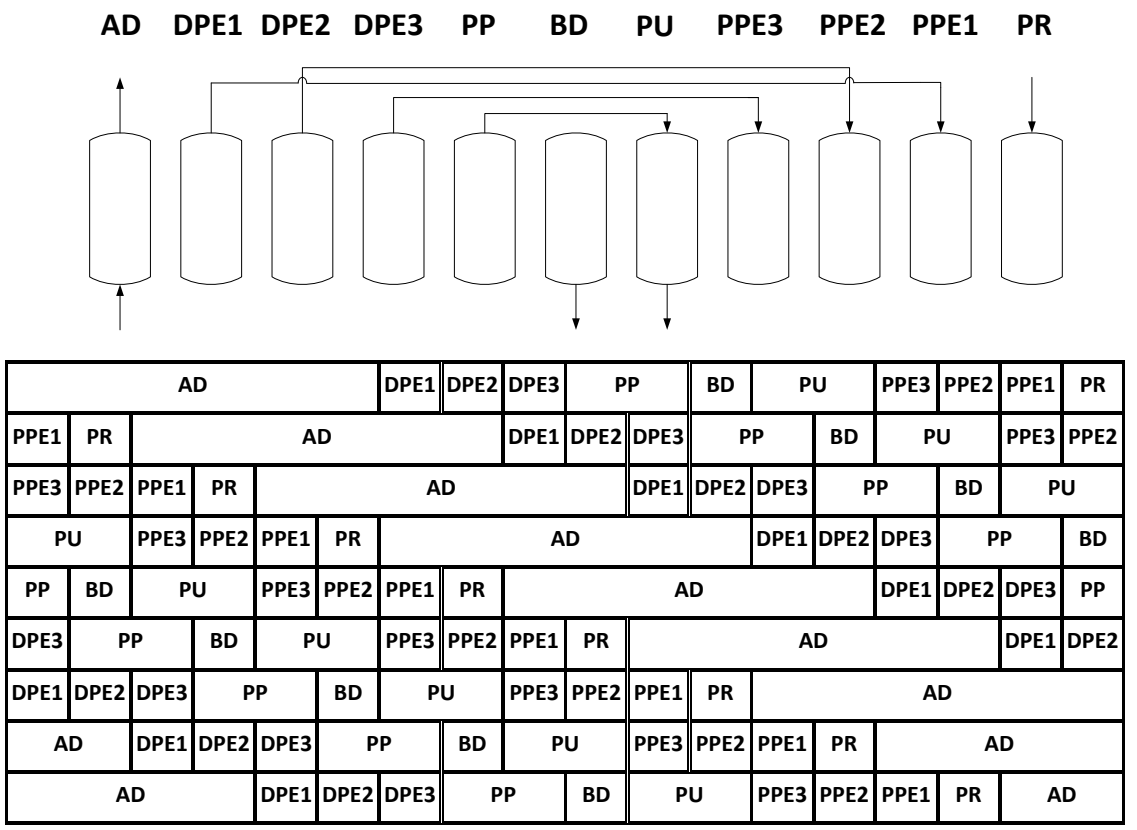

Figure 8. Step configurations of a nine-column PSA cycle (AD: Adsorption, DPE: Depressurising Pressure Equalisation, PP: Providing Purge, BD: Blowdown, PU: Purge, PPE: Pressurising Pressure Equalisation, PR: Pressurisation, $t_{AD} = t_{cycle}/3$; $t_{PP} = t_{PU} = t_{cycle}/9$; $t_{BD} = t_{DPE} = t_{PPE} = t_{PR} = t_{cycle}/18$).

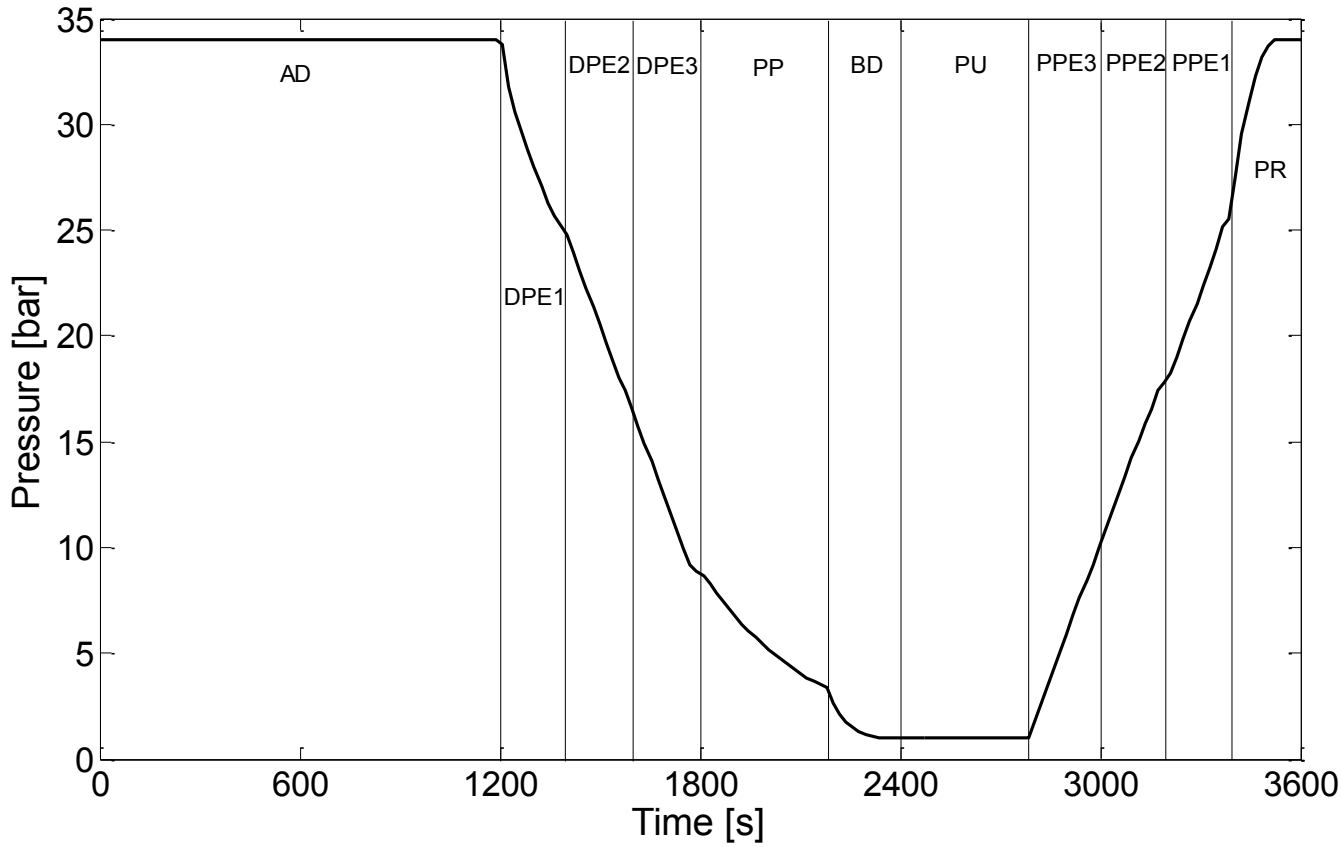

Figure 9. Pressure profiles at the product end of a column over a cycle at the cyclic steady state of a nine-column H_2 PSA at PP/F = 0.3.

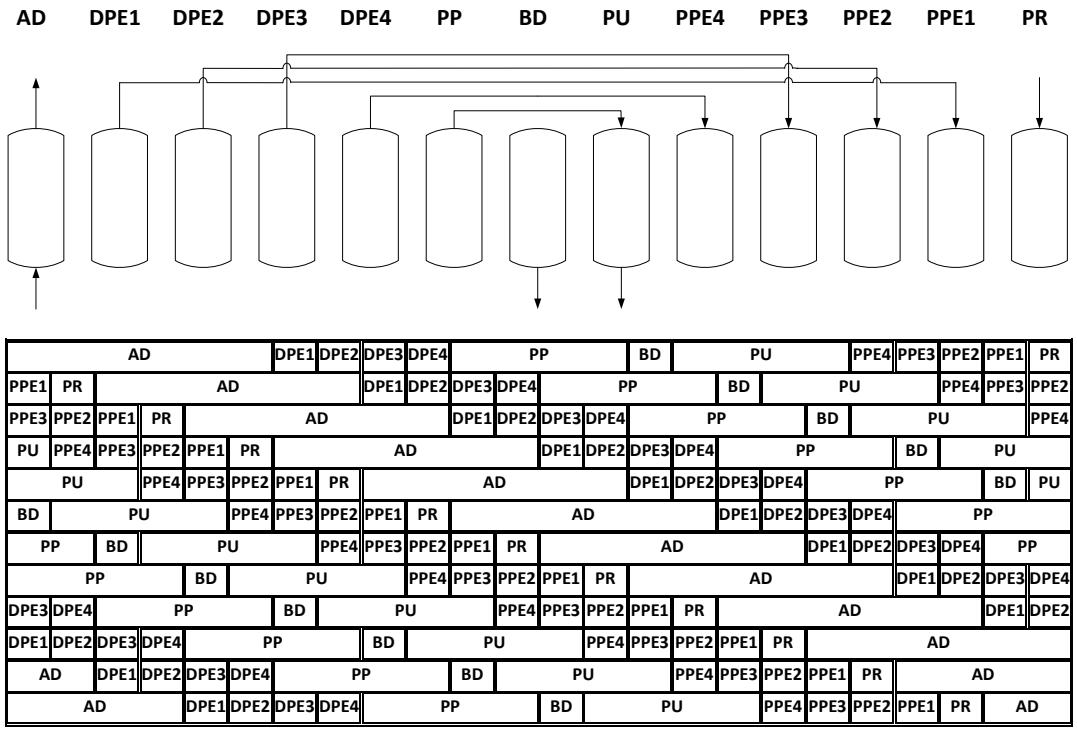

Figure 10. Step configurations of a twelve-column PSA cycle (AD: Adsorption, DPE: Depressurising Pressure Equalisation, PP: Providing Purge, BD: Blowdown, PU: Purge, PPE: Pressurising Pressure Equalisation, PR: Pressurisation, $t_{AD} = t_{cycle}/4$; $t_{PP} = t_{PU} = t_{cycle}/6$; $t_{BD} = t_{DPE} = t_{PPE} = t_{PR} = t_{cycle}/24$).

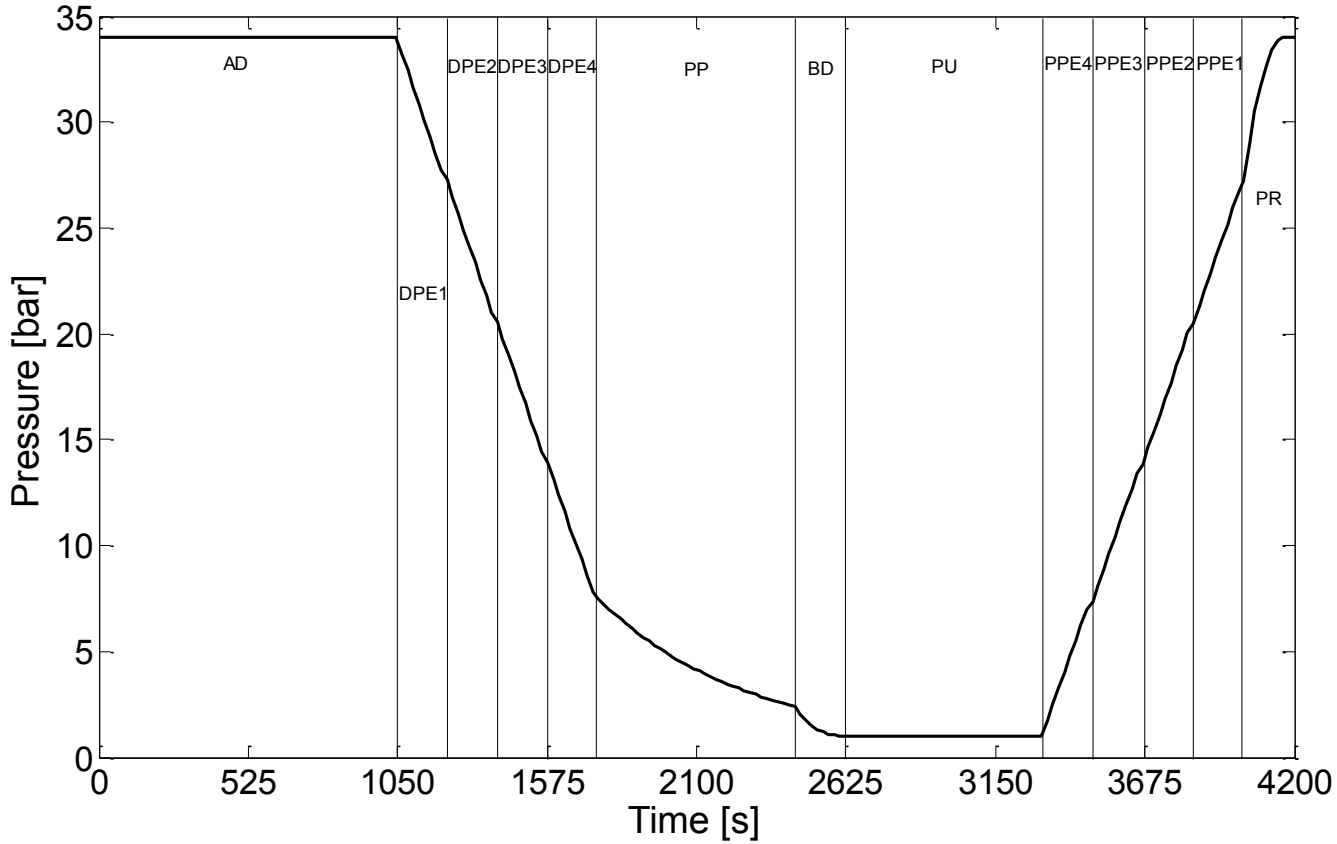

Figure 11. Pressure profiles at the product end of a column over a cycle at the cyclic steady state of a twelve-column H_2 PSA at PP/F = 0.3.

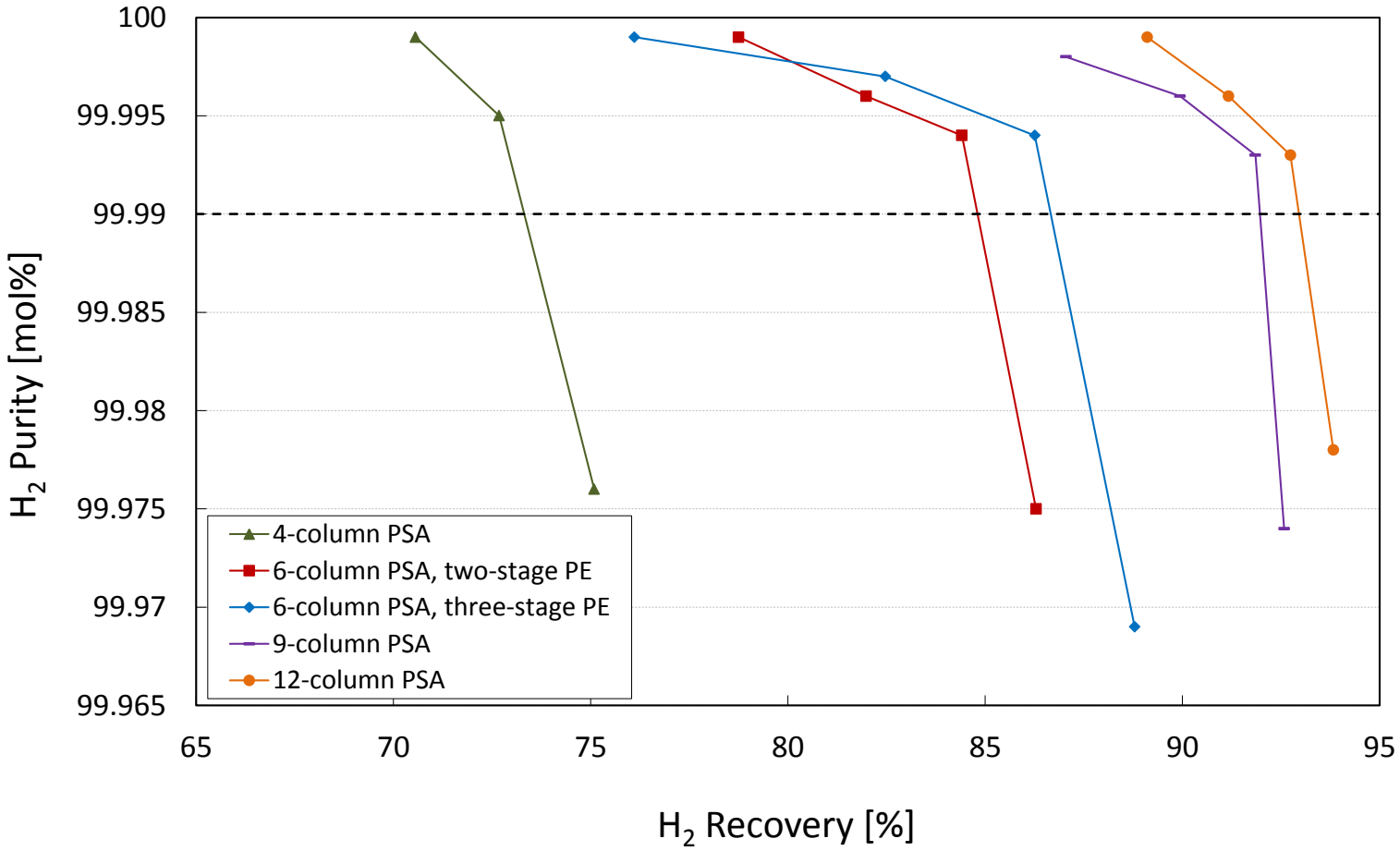

Figure 12. Comparison of hydrogen purity and recovery at various H_2 PSA systems with the different number of columns and different step configurations.

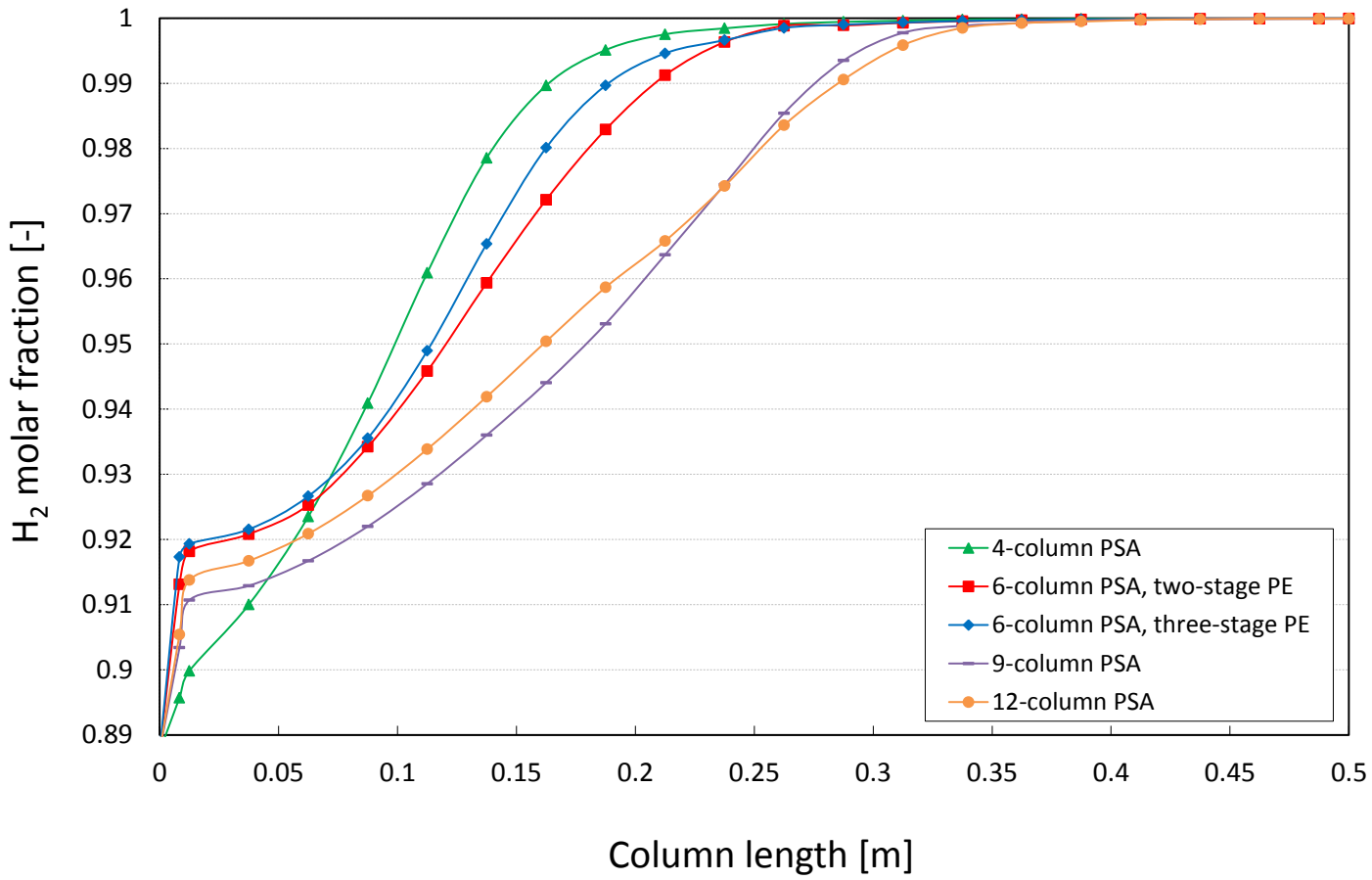

Figure 13. Hydrogen molar fraction profiles along the column at the end of the adsorption step in various PSA cycles at around 99.99% H_2 purity.